ROYAL SOCIETY
OF CHEMISTRY

PAPER

Check for updates

A highly oriented conductive MOF thin film-based Schottky diode for self-powered light and gas detection†

Lin-An Cao,[ac] Ming-Shui Yao,[b] Hui-Jie Jiang,[ac] Susumu Kitagawa, [b] Xiao-Liang Ye,[a] Wen-Hua Li[a] and Gang Xu [*ac]

The application of Schottky junction in self-powered devices is limited by low efficiency in both separation and transport of photogenerated electrons/holes. This issue may be overcome by introducing electronically conductive metal–organic framework (EC-MOF) materials into the junction and limited by preparing high-quality thin films of EC-MOFs. In this study, for the first time, high-quality EC-MOF thin films were demonstrated as effective interlayer materials to solve the above-mentioned issue by modulating the height of Schottky barrier (Φ_B). The EC-MOF-based self-powered Schottky diode can act as a photodetector and demonstrate the highest external quantum efficiency (84%) for all reported self-powered photodetectors as well as the broadest detectable spectrum range (250 to 1500 nm), high on–off ratio ($\sim 10^3$) and short rise (0.007 s) and fall time (0.03 s). Furthermore, it can be used as a gas sensor for typical harmful gases and vapors.

Introduction

Metal–organic frameworks (MOFs) or porous coordination polymers (PCPs) are a type of crystalline microporous materials that have shown considerable potential in gas-related applications, such as adsorption and storage, separation, catalysis, and sensing.[1–8] Moreover, MOFs are promising conductive materials owing to their crystalline and designable structures.[9–15] Through structural modulation, the well-known triphenylene-based electronically conductive MOFs (EC-MOFs) can vary their band gap from 0.58 to 0.85 eV and their conductivity from 10^{-6} to 40 S cm^{-1}.[16,17] Moreover, EC-MOFs are a type of rare crystalline materials possessing both conductive and microporous merits. Therefore, they have attracted considerable interest for electrical devices including electrocatalysts, supercapacitors, Li metal and Li ion batteries, field-effect transistors, thermoelectrical devices and chemi-resistive gas sensors.[18–24] However, numerous state-of-the-art EC-MOF-based electrical devices are in the form of powders, thick films, and non-oriented or microdomain-oriented thin films.[17,19,25–27] Therefore, the facile

[a] State Key Laboratory of Structural Chemistry, Fujian Institute of Research on the Structure of Matter, Chinese Academy of Sciences (CAS), 155 Yangqiao Road West, Fuzhou, Fujian, 350002, P. R. China. E-mail: gxu@firsm.ac.cn

[b] Institute for Integrated Cell-Material Sciences (WPI-iCeMS), Kyoto University Institute for Advanced Study, Kyoto University, Yoshida Ushinomiyacho, Sakyo-ku, Kyoto 606-8501, Japan

[c] University of Chinese Academy of Sciences (UCAS), No. 19A Yuquan Road, Beijing 100049, P. R. China

† Electronic supplementary information (ESI) available. See DOI: 10.1039/d0ta01379j

fabrication of an EC-MOF thin film with high orientation, controlled thickness and roughness is urgently required, although it still remains a challenge.

The Schottky junction forms at the interface of the metal and semiconductor and is very useful in photodetectors, solar cells, and biological/chemical sensors owing to the built-in electric field.[28–33] The performances of Schottky junction-based electrical devices are closely related to the height of Schottky barrier (Φ_B), which is the difference between the work function of metal electrodes and the electronic affinity of semiconductors.[29] Indeed, a higher Φ_B would provide a stronger built-in electric field and thus higher efficiency for promoting the separation of electron–hole pairs.[34–36] Theoretically, increasing the energy difference between the work function of the metal electrode and the electron affinity of the semiconductor can increase Φ_B. However, due to the Fermi pinning effect, Φ_B is insensitive to replacing metals with different work functions.[37,38] Alternatively, placing an interlayer material between the metal and semiconductor is an effective method to increase Φ_B. Several materials, such as graphene, MoO_3, MoS_2, and P3HT (poly(3-hexylthiophene-2,5-diyl)), have been demonstrated to be suitable for this purpose.[39–42] However, it is still very desirable to develop new interlayer materials, particularly the ones that can continuously tune their electronic structures to realize optimal performances of Schottky junction-based devices.

In this study, we propose that high-quality EC-MOF thin films, which possess flexibly tunable crystal and electronic structures are a type of effective interlayer materials for tuning the Φ_B of Schottky junctions. As a proof-of-concept, a series of triphenylene-based iso-structural EC-MOF thin films,

This journal is © The Royal Society of Chemistry 2020

J. Mater. Chem. A, 2020, **8**, 9085–9090 | **9085**

$M_3(C_{18}H_6X_6)_2$ (M = Ni or Cu; X = O or NH) were used to optimize the Si-based Schottky junction, which is known as one of the most important heterojunctions in a modern semiconductor technique. By varying the components in $M_3(C_{18}H_6X_6)_2$, Φ_B was continuously modulated from 0.67 eV in Ag/n-Si to 1.11 eV in Ag/EC-MOF/n-Si. Consequently, for the first time, a self-powered metal/n-Si Schottky diode was achieved by inserting a highly oriented, 20 nm-thick and low-roughness $Cu_3(C_{18}H_6(NH)_6)_2$ thin film. Without using any electric source, this device can act as a photodetector and show the highest external quantum efficiency (84%) in all reported self-powered photodetectors, the broadest detectable spectrum range (250–1500 nm), a high on–off ratio ($\sim10^3$), and a short rise (0.007 s) and fall time (0.03 s); moreover, it can be used as a gas sensor for typical harmful gases and vapors.

Results and discussion

Fig. 1 and S1† show the crystal structures of $M_3(C_{18}H_6X_6)_2$. These EC-MOFs are isostructural and possess interesting graphene-like honeycomb porous structures.[43] The preparation and characterizations of high-quality $Ni_3(C_{18}H_6(NH)_6)_2$ and $Cu_3(C_{18}H_6O_6)_2$ thin films have been reported in our previous studies and are shown in Fig. S2–S5.†[23,25] For the first time, the $Cu_3(C_{18}H_6(NH)_6)_2$ thin film was prepared *via* the LBL liquid-phase epitaxial method developed by Wöll *et al.*[44] First, the n-Si substrates were treated with a Piranha solution to functionalize –OH on their surfaces. Then, ethanol solution (0.1 mM) of copper(II) acetate and ethanol solution (0.01 mM) of 2,3,6,7,10,11-hexaaminotriphenylene were alternately sprayed on the functionalized substrates. In between, pure ethanol was used to rinse the substrates to get rid of unreacted reactants. The thickness of thin films was controlled by deposition cycles. $M_3(C_{18}H_6X_6)_2$ thin films with various thicknesses were denoted as $M_3(C_{18}H_6X_6)_2$-x nm (x is the thickness of the thin films). Ag/n-Si and Ag/$M_3(C_{18}H_6X_6)_2$/n-Si Schottky junctions were fabricated

by thermo-evaporating a 20 nm-thick Ag thin film on an n-Si wafer or $M_3(C_{18}H_6X_6)_2$/n-Si, respectively (Fig. 3a and S6†).

Fig. 2a, b and S2, S4, S6, and S7† show the top-view and cross-sectional view of the scanning electron microscopy (SEM) images of $M_3(C_{18}H_6X_6)_2$ thin films on Si substrates. The obtained films are homogeneous and continuous. Moreover, the thickness and roughness of the abovementioned films are characterized *via* atomic force microscopy (AFM) (Fig. 2c, S8 and S9†). Typically, it is observed that the thickness of the $Cu_3(C_{18}H_6(NH)_6)_2$ thin film linearly increases as deposition cycles increase and can be precisely controlled in averagely increasing 2 nm per cycle (Fig. 2d and S9†). The root mean square (RMS) roughness of a 20 nm-thick $Cu_3(C_{18}H_6(NH)_6)_2$ thin film is ~3 nm over a 100 μm^2 area, indicating a smooth surface (Fig. 2d). In UV-Vis absorption spectra, the absorbance of the $Cu_3(C_{18}H_6(NH)_6)_2$ thin film at 227 nm is linearly proportional to growth cycles, which further confirms its homogeneous growth (Fig. S10†). In Fourier transform infrared spectra, the typical peaks of the $Cu_3(C_{18}H_6(NH)_6)_2$-100 nm film (Fig. 2e) agree with those of the $Cu_3(C_{18}H_6(NH)_6)_2$ powder. As shown in Fig. 2f, both out-of-plane and in-plane patterns show obvious peaks that correspond very well to the peaks in the simulated pattern of $Cu_3(C_{18}H_6(NH)_6)_2$, except for the gap and background peaks from the detector.[22] However, the peaks from these two patterns are different from each other. The peak in the out-of-plane pattern is assigned to (00*l*), while all the peaks
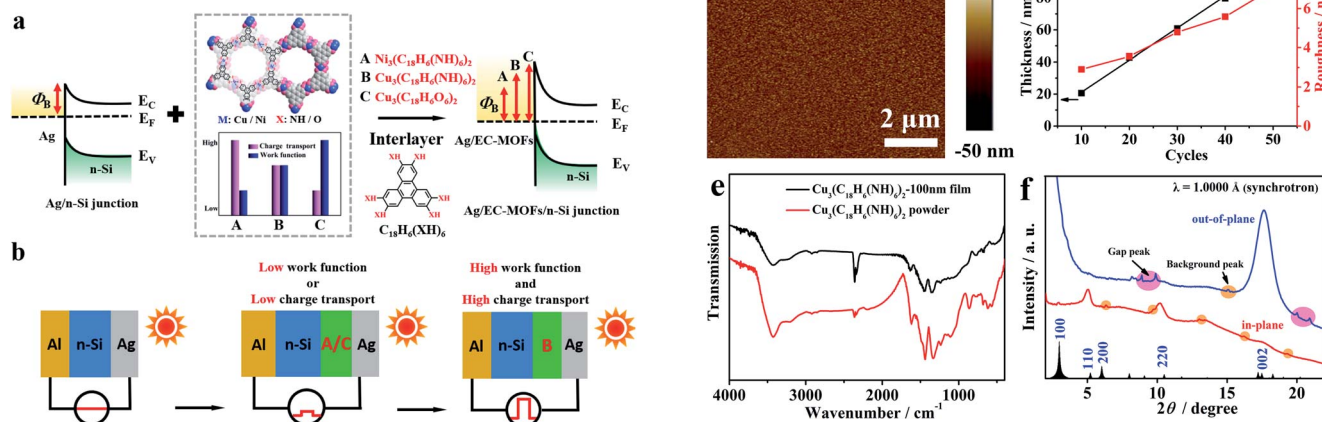

Fig. 1 (a) Energy band structure illustration of Ag/n-Si and Ag/EC-MOF/n-Si (within the dotted box are crystalline structure and electrical properties of EC-MOFs), (b) device construction and photoelectric performance illustration of Ag/EC-MOF/n-Si Schottky diodes.

Fig. 2 (a) Top view and (b) cross-sectional view HR-SEM, and (c) AFM image of the $Cu_3(C_{18}H_6(NH)_6)_2$-20 nm thin film, (d) growing cycle-dependent thickness and roughness of the $Cu_3(C_{18}H_6(NH)_6)_2$ thin film; (e) FTIR spectra of the $Cu_3(C_{18}H_6(NH)_6)_2$ powder and thin film; (f) GIXRD plots of $Cu_3(C_{18}H_6(NH)_6)_2$-20 nm.

9086 | *J. Mater. Chem. A*, 2020, **8**, 9085–9090

This journal is © The Royal Society of Chemistry 2020

in the in-plane pattern comprise those from (hk0). These observations suggest that the as-prepared $Cu_3(C_{18}H_6(NH_6)_6)_2$-20 nm is not only crystalline pure-phase $Cu_3(C_{18}H_6(NH)_6)_2$ but also highly oriented. The 1D channel in the crystal structure is perpendicular to the substrate.

According to the Mott–Schottky relation, a high work function of the electrode would result in a high Φ_B of the junction. Kelvin probe force microscopy (KPFM) measurements demonstrate that the work functions of EC-MOFs can be easily modulated by substituting their components and vary from 4.59 eV of $Ni_3(C_{18}H_6(NH)_6)_2$, to 4.69 eV of $Cu_3(C_{18}H_6(NH)_6)_2$, and then to 4.98 eV of $Cu_3(C_{18}H_6O_6)_2$. Pristine Ag has a work function of 4.23 eV; however, after decoration with 20 nm EC-MOFs, its work function is tuned to 4.29 eV for $Ag/Ni_3(C_{18}H_6(NH)_6)_2$, 4.38 eV for $Ag/Cu_3(C_{18}H_6(NH)_6)_2$ and 4.55 eV for $Ag/Cu_3(C_{18}H_6O_6)_2$ owing to the charge transfer between them[41] (for more details see Fig. 3b and S11 and S12†).

In order to deduce Φ_B, an Al electrode that can form ohmic contact with n-Si was evaporated on the back side of the as-prepared Schottky junctions to form Ag/n-Si/Al and Ag/EC-MOF-20 nm/n-Si/Al sandwich-structured diodes. Fig. 3c shows the I–V curves of these diodes, and typical rectifying characteristics are observed, indicating the existence of Schottky junctions in these devices. Φ_B can be calculated according to the thermionic emission theory model (for details see the ESI†).[28] The Φ_B of the Ag/n-Si junction remarkably increased from 0.67 to 0.92 eV after inserting EC-MOF-20 nm layers for $Ag/Ni_3(C_{18}H_6(NH)_6)_2$/n-Si, 0.95 eV for $Ag/Cu_3(C_{18}H_6(NH)_6)_2$/n-Si and 1.01 eV for $Ag/Cu_3(C_{18}H_6O_6)_2$/n-Si. Furthermore, this change in Φ_B is positively related to the change in the work function of EC-MOFs (Fig. 3d).

The Schottky junction diode has important applications in photo detection and gas sensing. However, its work mechanism

is very distinct compared with that of numerous nano-material-based photodetectors and gas sensors, such as InSe nanosheets, tellurium nanosheets and MoO_3 nanobelts.[46–48] Especially, Schottky junction diode can work possibly without power source, which reduces the device size, cost and energy consumption.[33,36,40,49,50] However, self-powered Schottky junction diodes are still limited by their low efficiency in the separation and transport of photo-induced electron/hole. Therefore, at a zero bias voltage, the Ag/n-Si/Al diode showed no response to light of any wavelength (Fig. 1b and S13a†). After inserting with an EC-MOFs-20 nm layer, this diode was endowed with self-powered photodetection ability due to significantly increased Φ_B and thus enhanced electron/hole separation efficiency (Fig. 4a and S13†). Compared with Ag/n-Si/Al, $Ag/Ni_3(C_{18}H_6(NH)_6)_2$/n-Si/Al shows an obvious response to light (Fig. S13b†). Its on–off ratio, responsivity (R_λ) and external quantum efficiency (EQE) are 2.2, 5 mA W^{-1} and 1.5% at a wavelength of 450 nm and a bias voltage of 0 V, respectively. Increasing Φ_B using $Cu_3(C_{18}H_6(NH)_6)_2$ produces considerably better photo sensing performances. $Ag/Cu_3(C_{18}H_6(NH)_6)_2$/n-Si/Al shows an on–off ratio of 533, an R_λ of 300 mA W^{-1} and an EQE of 84% at a wavelength of 450 nm (Fig. 4a). Notably, this
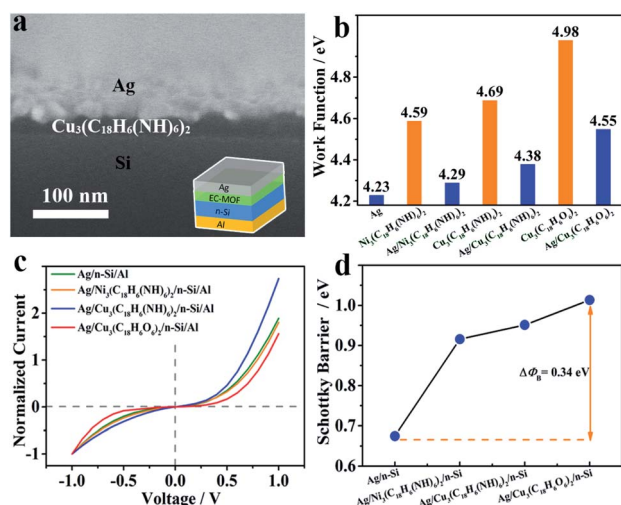
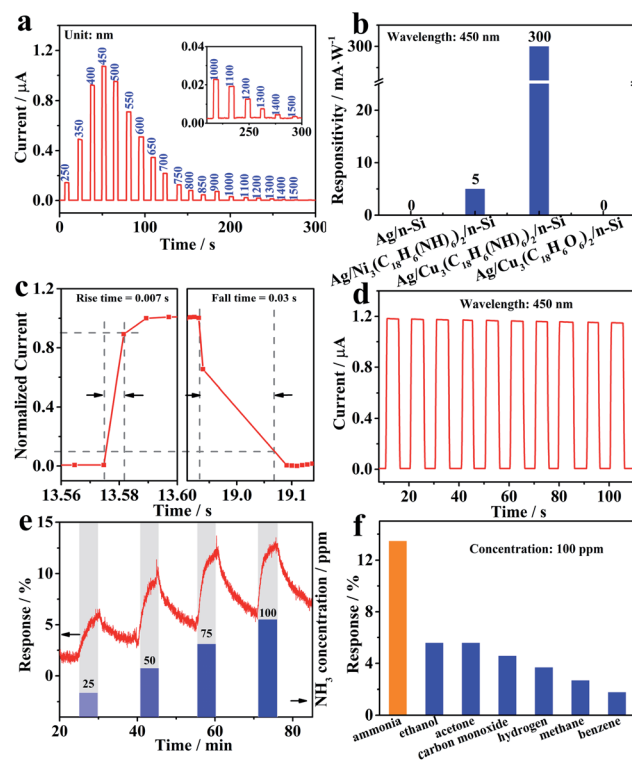**Fig. 4** (a) Wavelength-dependent photoresponse of $Ag/Ni_3(C_{18}H_6(NH)_6)_2$/n-Si/Al (inset: enlarged view at 1000–1500 nm); (b) comparison of the responsivity of different diodes; (c) normalized rise-fall time curve for $Ag/Cu_3(C_{18}H_6(NH)_6)_2$/n-Si/Al illuminated with 450 nm visible light at zero bias voltage; (d) photoresponse of $Ag/Cu_3(C_{18}H_6(NH)_6)_2$/n-Si/Al under 450 nm periodic illuminations; (e) response–recovery curves of $Ag/Cu_3(C_{18}H_6(NH)_6)_2$/n-Si/Al toward 25–100 ppm NH_3; (f) response of $Ag/Cu_3(C_{18}H_6(NH)_6)_2$/n-Si/Al diode toward different gases.

Fig. 3 (a) HR-SEM cross-section of the $Ag/Cu_3(C_{18}H_6(NH)_6)_2$/n-Si device (inset is device structure schematic); (b) work function of Ag, EC-MOFs and Ag/EC-MOFs; (c) Current–voltage plot of Ag/n-Si, $Ag/Ni_3(C_{18}H_6(NH)_6)_2$/n-Si, $Ag/Cu_3(C_{18}H_6N_6)_2$/n-Si, and $Ag/Cu_3(C_{18}H_6O_6)_2$/n-Si devices; (d) Schottky barrier height variation of different diodes.

This journal is © The Royal Society of Chemistry 2020

J. Mater. Chem. A, 2020, **8**, 9085–9090 | **9087**

EQE value is the highest one among all reported self-powered photodetectors, including Schottky junction type, p–n junction type and other heterojunctions (Table S1†). However, further increase in Φ_B using $Cu_3(C_{18}H_6O_6)_2$ results in almost no photosensing ability at a zero bias voltage (Fig. S13c†). This result reveals that in addition to the separation process, photosensing performances are determined by carrier transport. $Ag/Cu_3(C_{18}H_6(NH)_6)_2/n$-Si/Al has a series resistance (R_s) of 254 Ω (for details of the calculation see Fig. S14†). Comparatively, $Ag/Cu_3(C_{18}H_6O_6)_2/n$-Si/Al has a much higher R_s value of 31 254 Ω, indicating a worse carrier transport ability. A higher R_s would result in bad carrier transport, demonstrated by increase in the thickness of the EC-MOF layer from 20 to 40 nm in $Ag/Cu_3(C_{18}H_6(NH)_6)_2/n$-Si/Al. Hall measurement and impedance spectroscopy stud revealed that the carrier diffusion length in $Cu_3(C_{18}H_6(NH)_6)_2$ is 27.3 nm. Thus, the charge carrier can smoothly travel between the Ag thin film and n-Si *via* the 20 nm-thick $Cu_3(C_{18}H_6(NH)_6)_2$ layer (for more details see ESI and Fig. S15†). Although the device with a 40 nm-thick $Cu_3(C_{18}H_6(NH)_6)_2$ layer has Φ_B as high as 1.11 eV, this result discloses the reason why its R_s dramatically increased to 18 865 Ω and resulted in no obvious photo sensing performance at zero bias voltage (Fig. S13d and S14†).

With 20 nm-thick EC-MOF thin films, $Ag/Cu_3(C_{18}H_6(NH)_6)_2/n$-Si/Al shows the best self-powered sensing performance in our studied devices (Fig. 4b). As shown in Fig. 4c, it has a short rise and fall time with the value of 7 and 30 ms, respectively (for more details see Fig. 4c and ESI†). It can also be reversibly switched with little performance degradation for 10 cycles, indicating excellent stability and repeatability of our device (Fig. 4d). Moreover, this device has a high specific detectivity (D^*) of 3.2×10^{11} Jones. Further analysis on the photoresponse characteristics of the device under 450 nm illumination with different intensities reveals very low trap states existing in the device (for more details see Fig. S16†).[51]

The highly oriented porous structure of the $Cu_3(C_{18}H_6(NH)_6)_2$ layer that provides more accessible active sites for gas adsorption makes this diode very attractive to be used for gas sensing. To facilitate gas diffusion, the dense Ag thin film electrode in the device was replaced by a window-like Ag thin film (Fig. S17†). Under a 450 nm light, the current of $Ag/Cu_3(C_{18}H_6(NH)_6)_2/n$-Si/Al at zero bias voltage shows a response of 13.5% to 100 ppm NH_3; moreover, the response and recovery time are 2.4 and 7.5 min, respectively (Fig. 4e). In the range of 25–100 ppm NH_3, this device has good linear log–log plots of response and concentration (Fig. S15b†), indicating a quantitative detection potential. Moreover, this device has good repeatability with a coefficient of variation as low as 3.4% in five continuous test cycles to 100 ppm NH_3. Furthermore, this device shows good selectivity to NH_3 compared with the other five commonly existed interfering gases (Fig. 4f). It is expected to be used as a part of the sensor array in the electronic nose to get better selectivity to distinguish different gases. The long-term stability of $Ag/Cu_3(C_{18}H_6(NH)_6)_2/n$-Si/Al is shown in Fig. S18† and requires further improvement by material optimization or device packaging in future.

Conclusions

In conclusion, for the first time, highly oriented, ultra-thin, and low-roughness EC-MOF thin film was prepared and demonstrated as an effective interlayer material to modulate the height of the Schottky barrier. Consequently, this Schottky junction-based diode effectively enhanced its separation efficiency in photo-generated electron/hole pairs through enhanced built-in electrical field, which can even afford a self-powered device operation. Compared with other self-powered photodetectors, this diode achieved the highest external quantum efficiency (84%), broadest detectable spectrum range (250 nm to 1500 nm), high on–off ratio ($\sim10^3$) as well as short rise (0.007 s) and fall time (0.03 s). Moreover, taking the advantage of the porous structure of EC-MOFs, this diode demonstrated gas sensing ability to typical harmful gases and vapors. This study provides both a new type of materials for improving the performances of the Schottky junction and developes a new application for MOFs in self-powered devices.

Experimental

Characterization

All reagents were commercially purchased and used without further purification. Copper acetate ($Cu(OAc)_2 \cdot H_2O$) was purchased from Sinopharm Group Co., Ltd. (China). HITP (2,3,6,7,10,11-hexaaminotriphenylene) ligand was purchased from WuXi Apptec Co., Ltd. (China). HHTP (2,3,6,7,10,11-hexahydroxytriphenylene) ligand was purchased from TCI (Shanghai). The morphologies of thin films were observed by scanning electron microscopy (SEM) images, which were obtained using JSM6700-F operating at 1.5 kV. The thickness and roughness of thin films were obtained by atomic force microscopy (AFM), which was performed using Bruker Dimension Icon in tapping mode. $Cu_3(C_{18}H_6(NH)_6)_2$ thin films growing on quartz substrates were then used for UV-vis spectrum measurements using Perkin-Elmer Lambda 900. The grazing incidence X-ray diffraction (GIXRD) was performed using BL46XU, SPring-8 in Japan. The X-ray wavelength was 1.0000 Å; the incident angle for the in-plane diffraction was 0.12; and the exposed time was 20 s. The Fourier transform infrared (FTIR) spectra were recorded on a Bruker VERTEX70 FT-IR spectrometer (Germany) in the 4000–400 cm^{-1} region using KBr pellets. Work function measurements were executed on Kelvin probe force microscopy (KPFM) using Bruker Dimension Icon in tapping mode by measuring the local variation of the surface potential. The reference was HOPG (work function is 4.48 eV)[45] and the measurements were collected in air at room temperature. Hall test was performed on an 8404 Hall Effect System of Lake Shore company.

Functionalization of substrates

Si substrates were ultrasonically washed with DI water, acetone and ethanol for 10 min, respectively. They were then immersed in a Piranha solution (H_2SO_4 (95–98%) : H_2O_2 (30%) = 7 : 3) at 100 °C for 1 h, and then rinsed and ultrasonically washed in DI

9088 | *J. Mater. Chem. A*, 2020, **8**, 9085–9090

This journal is © The Royal Society of Chemistry 2020

water for 10 min. Furthermore, the substrates were dried by N_2 flux before use.

Preparation of $Ni_3(C_{18}H_6(NH)_6)_2$ thin films

10.0 mg (0.019 mmol) of HITP and 6.6 mg (0.028 mmol) of nickel chloride hexahydrate ($NiCl_2 \cdot 6H_2O$) were dissolved in 20.0 mL of DI water. The reaction mixture was then sonicated until the solids were completely dissolved. Then, the reaction mixture was heated to 65 °C and 0.3 mL of ammonium hydroxide was added. Black-blue thin films were observed at the air/liquid interface. The 20 nm-thick thin film was obtained by extending the reaction time to ~90 s.

Preparation of $Cu_3(C_{18}H_6(NH)_6)_2$ thin films

$Cu_3(C_{18}H_6(NH)_6)_2$ thin films were fabricated on functionalized n-Si substrates using the layer-by-layer liquid-phase epitaxy (LBL) spray method as has been reported previously.[25] The substrates were fixed on a sample holder and then sprayed with $Cu(OAc)_2 \cdot H_2O$ (0.1 mM) in ethanol for 20 s and then with solution of HITP ligand (0.01 mM) in ethanol for 40 s at room temperature. The pH value of the solution of HITP ligand was regulated to 8.5 by ammonium hydroxide (28%). In between, the thin films were rinsed by spraying pure ethanol for 20 s to remove the unreacted reactants, and then dried by N_2. By controlling the number of deposition cycles, the 20–100 nm-thick $Cu_3(C_{18}H_6(NH)_6)_2$ thin films were successfully fabricated.

Preparation of the $Cu_3(C_{18}H_6O_6)_2$ thin film

The preparation process of the $Cu_3(C_{18}H_6O_6)_2$ thin film was the same as that of $Cu_3(C_{18}H_6(NH)_6)_2$, except that the ligand was HHTP without ammonium hydroxide. The 20 nm-thick $Cu_3(C_{18}H_6O_6)_2$ thin film was obtained after ten deposition cycles.

Preparation of $Cu_3(C_{18}H_6(NH)_6)_2$ powders

$Cu_3(C_{18}H_6(NH)_6)_2$ powders were synthesized using the method reported by Dincă et al.[22] 7 mg (0.028 mmol) of $CuSO_4 \cdot 5H_2O$ and 75 μL of $NH_3 \cdot H_2O$ were added into 2 mL DI water. Moreover, 10 mg (0.019 mmol) of the HITP ligand was added into 2 mL DI water. These two solutions were then mixed together at room temperature and immediately a black precipitate was formed. After stirring for 3 h, the products were collected from the reactor and washed for three times with DI water and ethanol, respectively. Then, the black compounds were dried in vacuum at 60 °C for 12 h.

Preparation of Ag/EC-MOFs/n-Si/Al photodetector and gas sensing devices

A commercial n-type Si (100) wafer was used as a substrate to construct Ag/n-Si/Al and Ag/EC-MOFs/n-Si/Al Schottky diode devices. First, a Ag electrode (0.5 mm × 0.5 mm) was thermally evaporated on the surface of n-type Si with a shadow mask to form Schottky junction. In order to ensure that light penetrates as much as possible, the thickness of semitransparent Ag electrode was ~20 nm. For the devices with the interlayer, EC-

MOF thin films were deposited on the surface of n-Si by the air/liquid interface method or LBL liquid phase epitaxial spray method before the evaporation of the Ag electrode. The EC-MOF thin films outside the electrode area were then removed by an ethanol-dipped cotton swab. Then, the Al electrode (about 50 nm) was deposited by thermal evaporation on the back side of the n-Si substrate.

Photo detection and gas sensing measurements

Photo detection measurements were performed on a Keithley 4200 SCS semiconductor parameter analyzer and Lake shore probe station. A Quanta Master fiber optic spectrometer was then used as the light source. The gas sensing measurements were conducted using a home-made system reported in our previous work.[52,53] Moreover, the target gas was introduced into the quartz tube by mixing the certified gas (Beijing HuaYuan Gas Chemical Industry Co., Ltd., China) and dry air in a proper ratio and controlled by the mass flow controllers (CS–200C, Beijing Sevenstar Qualiflow Electronic Equipment Manufacturing Co., Ltd., China). The constant flow was 600 mL min^{-1}, the bias on the sensing device was 0 V and the current was recorded using a Keithley 2602B source meter. The light source for gas sensing test was PLS-SXE300C xenon lamp with a band pass filter of 450 nm.

Conflicts of interest

There are no conflicts to declare.

Acknowledgements

References

1 S. Horike, S. S. Nagarkar, T. Ogawa and S. Kitagawa, Angew. Chem., Int. Ed., 2020, 59, 6652–6664.

2 B. Wang, A. P. Cote, H. Furukawa, M. O'Keeffe and O. M. Yaghi, Nature, 2008, 453, 207–211.

3 R. Haldar, L. Heinke and C. Wöll, Adv. Mater., 2019, 1905227.

4 K. Jayaramulu, F. Geyer, A. Schneemann, S. Kment, M. Otyepka, R. Zboril, D. Vollmer and R. A. Fischer, Adv. Mater., 2019, 31, e1900820.

5 J. R. Li, R. J. Kuppler and H. C. Zhou, Chem. Soc. Rev., 2009, 38, 1477–1504.

6 I. Stassen, N. Burtch, A. Talin, P. Falcaro, M. Allendorf and R. Ameloot, Chem. Soc. Rev., 2017, 46, 3185–3241.

7 X. Fang, Q. Shang, Y. Wang, L. Jiao, T. Yao, Y. Li, Q. Zhang, Y. Luo and H. L. Jiang, Adv. Mater., 2018, 30, 1705112.

This journal is © The Royal Society of Chemistry 2020

J. Mater. Chem. A, 2020, 8, 9085–9090 | 9089

8 L. Jiao, Y. Wang, H. L. Jiang and Q. Xu, *Adv. Mater.*, 2018, **30**, e1703663.

9 M. K. Smith, K. E. Jensen, P. A. Pivak and K. A. Mirica, *Chem. Mater.*, 2016, **28**, 5264–5268.

10 L. Sun, M. G. Campbell and M. Dincă, *Angew. Chem., Int. Ed.*, 2016, **55**, 3566–3579.

11 G. Skorupskii, B. A. Trump, T. W. Kasel, C. M. Brown, C. H. Hendon and M. Dincă, *Nat. Chem.*, 2020, **12**, 131–136.

12 C. Schneider, D. Ukaj, R. Koerver, A. A. Talin, G. Kieslich, S. P. Pujari, H. Zuilhof, J. Janek, M. D. Allendorf and R. A. Fischer, *Chem. Sci.*, 2018, **9**, 7405–7412.

13 Y. Yoshida, K. Fujie, D. W. Lim, R. Ikeda and H. Kitagawa, *Angew. Chem., Int. Ed.*, 2019, **58**, 10909–10913.

14 X. Jiang, L. Zhang, S. Liu, Y. Zhang, Z. He, W. Li, F. Zhang, Y. Shi, W. Lue, Y. Li, Q. Wen, J. Li, J. Feng, S. Ruan, Y. J. Zeng, X. Zhu, Y. Lu and H. Zhang, *Adv. Opt. Mater.*, 2018, **6**, 1800561.

15 Z. Sun, X. Jiang, Q. Wen, W. Li and H. Zhang, *J. Mater. Chem. C*, 2019, **7**, 4662–4666.

16 X. Song, X. Wang, Y. Li, C. Zheng, B. Zhang, C.-a. Di, F. Li, C. Jin, W. Mi, L. Chen and W. Hu, *Angew. Chem., Int. Ed.*, 2020, **59**, 1118–1123.

17 D. Sheberla, L. Sun, M. A. Blood-Forsythe, S. Er, C. R. Wade, C. K. Brozek, A. Aspuru-Guzik and M. Dinca, *J. Am. Chem. Soc.*, 2014, **136**, 8859–8862.

18 W. H. Li, K. Ding, H. R. Tian, M. S. Yao, B. Nath, W.-H. Deng, Y. Wang and G. Xu, *Adv. Funct. Mater.*, 2017, **27**, 1702067.

19 M. G. Campbell, S. F. Liu, T. M. Swager and M. Dinca, *J. Am. Chem. Soc.*, 2015, **137**, 13780–13783.

20 W. H. Li, J. Lv, Q. Li, J. Xie, N. Ogiwara, Y. Huang, H. Jiang, H. Kitagawa, G. Xu and Y. Wang, *J. Mater. Chem. A*, 2019, **7**, 10431–10438.

21 D. Sheberla, J. C. Bachman, J. S. Elias, C. J. Sun, Y. Shao-Horn and M. Dincă, *Nat. Mater.*, 2017, **16**, 220–224.

22 M. G. Campbell, D. Sheberla, S. F. Liu, T. M. Swager and M. Dincă, *Angew. Chem., Int. Ed.*, 2015, **54**, 4349–4352.

23 G. Wu, J. Huang, Y. Zang, J. He and G. Xu, *J. Am. Chem. Soc.*, 2017, **139**, 1360–1363.

24 M. S. Yao, J. W. Xiu, Q. Q. Huang, W. H. Li, W. W. Wu, A. Q. Wu, L. A. Cao, W. H. Deng, G. E. Wang and G. Xu, *Angew. Chem., Int. Ed.*, 2019, **58**, 14915–14919.

25 M. S. Yao, X. J. Lv, Z. H. Fu, W. H. Li, W. H. Deng, G. D. Wu and G. Xu, *Angew. Chem., Int. Ed.*, 2017, **56**, 16510–16514.

26 H. Maeda, R. Sakamoto and H. Nishihara, *Langmuir*, 2016, **32**, 2527–2538.

27 T. Kambe, R. Sakamoto, K. Hoshiko, K. Takada, M. Miyachi, J. H. Ryu, S. Sasaki, J. Kim, K. Nakazato, M. Takata and H. Nishihara, *J. Am. Chem. Soc.*, 2013, **135**, 2462–2465.

28 X. Li, H. Zhu, K. Wang, A. Cao, J. Wei, C. Li, Y. Jia, Z. Li, X. Li and D. Wu, *Adv. Mater.*, 2010, **22**, 2743–2748.

29 A. Di Bartolomeo, *Phys. Rep.*, 2016, **606**, 1–58.

30 X. Zhao, R. Zhou, Q. Hua, L. Dong, R. Yu and C. Pan, *J. Nanomater.*, 2015, **2015**, 1–20.

31 R. Paolesse, S. Nardis, D. Monti, M. Stefanelli and C. Di Natale, *Chem. Rev.*, 2016, **117**, 2517–2583.

32 C. Y. Wu, Z. Q. Pan, Y. Y. Wang, C. W. Ge, Y.-Q. Yu, J. Y. Xu, L. Wang and L.-B. Luo, *J. Mater. Chem. C*, 2016, **4**, 10804–10811.

33 D. Lee, H. Park, S. D. Han, S. H. Kim, W. Huh, J. Y. Lee, Y. S. Kim, M. J. Park, W. I. Park, C. Y. Kang and C. H. Lee, *Small*, 2019, **15**, e1804303.

34 L. Han, X. Zhao, M. Ma, F. Gao, X. Xun, Q. Liao, Z. Zhang, Z. Kang and Y. Zhang, *Nano Energy*, 2019, **57**, 528–534.

35 A. A. M. Farag, A. Ashery, E. M. A. Ahmed and M. A. Salem, *J. Alloys Compd.*, 2010, **495**, 116–120.

36 L. Su, W. Yang, J. Cai, H. Chen and X. Fang, *Small*, 2017, **13**, 1701687.

37 D. J. Chadi, P. H. Citrin, C. H. Park, D. L. Adler, M. A. Marcus and H. J. Gossmann, *Phys. Rev. Lett.*, 1997, **79**, 4834–4837.

38 A. Dimoulas, P. Tsipas, A. Sotiropoulos and E. K. Evangelou, *Appl. Phys. Lett.*, 2006, **89**, 252110.

39 H. Yu, M. Schaekers, T. Schram, S. Demuynck, N. Horiguchi, K. Barla, N. Collaert, A. V. Y. Thean and K. De Meyer, *IEEE Trans. Electron. Devices*, 2016, **63**, 2671–2676.

40 D. Xiang, C. Han, Z. Hu, B. Lei, Y. Liu, L. Wang, W. P. Hu and W. Chen, *Small*, 2015, **11**, 4829–4836.

41 C. Xie, X. Zhang, Y. Wu, X. Zhang, X. Zhang, Y. Wang, W. Zhang, P. Gao, Y. Han and J. Jie, *J. Mater. Chem. A*, 2013, **1**, 8567.

42 K. Ding, X. Zhang, F. Xia, R. Wang, Y. Kuang, S. Duhm, J. Jie and X. Zhang, *J. Mater. Chem. A*, 2017, **5**, 285–291.

43 M. Hmadeh, Z. Lu, Z. Liu, F. Gándara, H. Furukawa, S. Wan, V. Augustyn, R. Chang, L. Liao, F. Zhou, E. Perre, V. Ozolins, K. Suenaga, X. Duan, B. Dunn, Y. Yamamto, O. Terasaki and O. M. Yaghi, *Chem. Mater.*, 2012, **24**, 3511–3513.

44 H. K. Arslan, O. Shekhah, J. Wohlgemuth, M. Franzreb, R. A. Fischer and C. Wöll, *Adv. Funct. Mater.*, 2011, **21**, 4228–4231.

45 J. Meyer, R. Khalandovsky, P. Gorrn and A. Kahn, *Adv. Mater.*, 2011, **23**, 70–73.

46 S. Yang, Y. Liu, W. Chen, W. Jin, J. Zhou, H. Zhang and G. S. Zakharova, *Sens. Actuators, B*, 2016, **226**, 478–485.

47 Z. Li, H. Qiao, Z. Guo, X. Ren, Z. Huang, X. Qi, S. C. Dhanabalan, J. S. Ponraj, D. Zhang, J. Li, J. Zhao, J. Zhong and H. Zhang, *Adv. Funct. Mater.*, 2018, **28**, 1705237.

48 Z. Xie, C. Xing, W. Huang, T. Fan, Z. Li, J. Zhao, Y. Xiang, Z. Guo, J. Li, Z. Yang, B. Dong, J. Qu, D. Fan and H. Zhang, *Adv. Funct. Mater.*, 2018, **28**, 1705833.

49 K. Deng and L. Li, *Adv. Mater.*, 2014, **26**, 2619–2635.

50 A. I. Nusir, S. J. Bauman, M. S. Marie, J. B. Herzog and M. O. Manasreh, *Appl. Phys. Lett.*, 2017, **111**, 171103.

51 S. Chen, X. Liu, X. Qiao, X. Wan, K. Shehzad, X. Zhang, Y. Xu and X. Fan, *Small*, 2017, **13**, 1604033.

52 M. S. Yao, W. X. Tang, G. E. Wang, B. Nath and G. Xu, *Adv. Mater.*, 2016, **28**, 5229–5234.

53 M. S. Yao, L. A. Cao, Y. X. Tang, G. E. Wang, R. H. Liu, P. N. Kumar, G. D. Wu, W. H. Deng, W. J. Hong and G. Xu, *J. Mater. Chem. A*, 2019, **7**, 18397–18403.

9090 | *J. Mater. Chem. A*, 2020, **8**, 9085–9090

This journal is © The Royal Society of Chemistry 2020